The formation of cylindrical aggregates plays an important role in the percolation transition. The locus of the percolation threshold at high salinity hits the critical point $\phi_{BS,UC}$ (Figure 4a). The shape of aggregates has an effect on both the percolation threshold and the phase separation. Thus, the difference in the shape of aggregates between the SDEHP and AOT case is essential for the difference in phase diagrams for both systems.

The interaggregate interaction is important for the phase diagram of microemulsion but is not discussed here due to the lack of further experimental information.

Conclusions

The phase equilibrium of sodium bis(2-ethylhexyl) phosphate (SDEHP)/water/*n*-heptane/sodium chloride microemulsion was examined at 25.0 °C. The effect of the NaCl concentrations in the excess aqueous phase on the microemulsion phase was examined in detail. The range of NaCl concentrations where three phases coexist was much wider than that for AOT/water/*n*-heptane/sodium chloride microemulsion at the same temperature. Cylindrical aggregates were found to exist in the oil-rich region in SDEHP system. In the brine-rich region, the disklike aggregates were predominant. The middle phase was found to be also composed of these microstructures. The phase boundaries between the microemulsion phase and the excess organic phase were independent of the salinity condition in the oil-rich region. The formation of the middle phase was similar to the gas–liquid phase transition at low salinity and was closely related to the formation of cylindrical network at high salinity. The difference in the shape of aggregates between SDEHP and AOT cases plays an important role for the difference in their phase diagrams.

Acknowledgment. We gratefully acknowledge the financial support from a Grant in Aid for Fundamental Scientific Research, Ministry of Education, Culture and Science, Japan.

Registry No. SDEHP, 141-65-1; NaCl, 7647-14-5; $H_3C(CH_2)_5CH_3$, 142-82-5.

Small-Angle Neutron Scattering from Diffuse Interfaces. 1. Mono- and Bilayers in the Water–Octane–$C_{12}E_5$ System

R. Strey,* J. Winkler,

Max Planck Institut für Biophysikalische Chemie, Postfach 2841, 3400 Göttingen, FRG

and L. Magid

Department of Chemistry, University of Tennessee, Knoxville, Tennessee 37996-1600
(Received: March 1, 1991)

We have investigated the small-angle neutron scattering (SANS) of ternary microemulsions and a binary L_3 phase. Of particular interest is the local structure of monolayers at the water–oil interface in microemulsions and of bilayers in the isotropic anomalous L_3 phase of the binary water–nonionic surfactant system. In both cases the scattering is characteristic of a locally flat structure with a diffuse interface which arises from the penetration of solvent molecules. We interpret the data in terms of a Gaussian scattering length density profile which varies smoothly across the mono- and bilayers. From the scattering curves we obtain the width of the layers and the effective areas occupied by the surfactant molecules. Furthermore, we conclude that for the case of bilayers the hydrophobic tails of the surfactant molecules in the opposing monolayers interdigitate.

Introduction

We are currently investigating the local structure of water, oil, and surfactant mixtures. In such systems the surfactant molecules may form extended self-connected layers[1] separating hydrophilic from hydrophobic domains. Examples are bicontinuous microemulsions and L_3 phases.

In the bicontinuous microemulsion, a multiply connected randomly oriented *monolayer* separates water- and oil-rich subvolumes. Both the oil and the water domains are continuous, as evidenced by NMR self-diffusion experiments on the system studied here and on related systems.[2,3] With freeze fracture electron microscopy (FFEM) one observes water and oil domains forming an interpenetrating network.[4]

In the L_3 phase a multiply connected randomly oriented *bilayer* is found to divide space into two equivalent water-continuous subvolumes.[5-8]

Experimental studies and theoretical considerations[9-13] support the notion that the microstructure of both types of phases are topologically similar. The theoretical explanations for such structures involve interfacial tension and bending energy arguments. To give a visual impression we show in Figure 1 an artist's impression of a structural element (first suggested by Porte et al.,[5] later modified by Strey et al.[8]) of the local mono- or bilayer structure of the amphiphilic film as consistent with FFEM pictures[4,8] and supported by theory.[5,9,10,13]

We measured the small-angle neutron scattering (SANS) of the L_3 phase in the binary water–$C_{12}E_5$ system and of bicontinuous microemulsions in the ternary water–*n*-octane–$C_{12}E_5$ system. We

* To whom correspondence should be addressed.

(1) Roux, D.; Cates, M. *Proc. 4th Nishinomiya-Yukawa Symp. Springer* **1989**.
(2) Kahlweit, M.; Strey, R.; Haase, D.; Kunieda, H.; Schmeling, T.; Fauhlhaber, B.; Borkovec, M.; Eicke, H.-F.; Busse, G.; Eggers, F.; Funck, Th.; Richmann, H.; Magid, L.; Söderman, O.; Stilbs, P.; Winkler, J.; Dittrich, A.; Jahn, W. *J. Colloid Interface Sci.* **1987**, *118*, 436.
(3) Olsson, U.; Shinoda, K.; Lindman, B. *J. Phys. Chem.* **1986**, *90*, 4083.
(4) Jahn, W.; Strey, R. *J. Phys. Chem.* **1988**, *92*, 2294.
(5) Porte, G.; Marignan, J.; Bassereau, P.; May, R. *J. Phys. Fr.* **1988**, *49*, 511.
(6) Gazeau, D.; Bellocq, A. M.; Zemb, T.; Roux, D. *Europhys. Lett.* **1989**, *9*, 447.
(7) Strey, R.; Schomäcker, R.; Nallet, F.; Roux, D.; Olsson, U. *J. Chem. Soc., Faraday Trans.* **1990**, *86*, 2253.
(8) Strey, R.; Jahn, W.; Porte, G.; Bassereau, P. *Langmuir* **1990**, *6*, 1635.
(9) Milner, S. T.; Safran, S. A.; Cates, M. E.; Andelman, D.; Roux, D. *J. Phys. Fr.* **1988**, *49*, 1065.
(10) Cates, M. E.; Roux, D.; Andelman, D.; Milner, S. T.; Safran, S. A. *Europhys. Lett.* **1988**, *5*, 733.
(11) Huse, D. A.; Leibler, S. *J. Phys. Fr.* **1988**, *49*, 605.
(12) Anderson, D. M.; Wennerström, H.; Olsson, U. *J. Phys. Chem.* **1989**, *93*, 4243.
(13) Anderson, D. M.; Wennerström, H. *J. Phys. Chem.* **1990**, *94*, 8683.

0022-3654/91/2095-7502$02.50/0

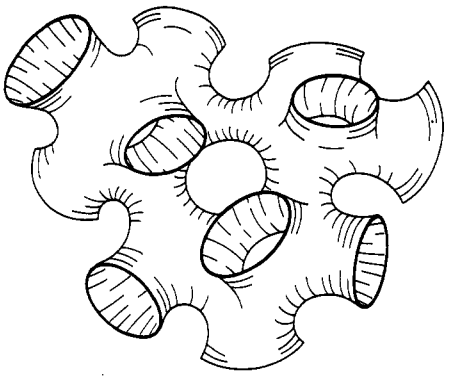

Figure 1. Schematic picture of a structural element of the monolayer in a bicontinuous microemulsion or of the bilayer in the L_3 phase consistent with a variety of experimental results like electrical conductivity,[5] NMR self-diffusion,[2,3,26] freeze fracture electron microscopy pictures,[8] and theoretical predictions.[9-13]

chose this system because its phase behavior is well known[2,7] and it has been studied by several complementary techniques.

Here, we show that the scattering of the monolayers in the bicontinuous microemulsions and the bilayers is closely related. Scattering spectra on an absolute scale permit a qualitative analysis yielding numbers for the effective area of the surfactant molecules in the amphiphilic film.

Theoretical Considerations

The surfactant molecules form a 2-D film, a monolayer in the microemulsions and a bilayer in the L_3 phase, penetrated to some extent by the surrounding solvents. To start with we assume that all surfactant molecules aggregate to form the total area of the internal surface per unit volume $A = S/V$. One has $A = \nu a_S \phi_S / 2 v_s$ with $\nu = 1$ and 2 for a bilayer and for a monolayer, respectively, because $\phi_s = v_s N_s / V$ and $S = \nu a_s N_s / 2$. The effective thickness δ of the (thin) surface is set by the surfactant volume fraction and the internal surface area, $\delta = \phi_s / A$. For v_s one may set in sufficient approximation $v_s = M/\rho_s N_A$. The effective area per surfactant molecule a_s, however, is determined by the energetics of the system and may accordingly vary depending on the respective state (e.g., temperature, nature of the oil, etc.).

Scattering from a Diffuse 2-D Film. One of the most useful features of small-angle neutron scattering is the possibility of contrast variation. If one matches the contrast of the liquids on both sides of the film one picks up scattering from the film only. It is evident that in such cases the scattering intensity will be the larger the larger the total amount of surface and the higher the contrast between film and surrounding bulk. The amplitude F of the scattering is proportional to the difference in scattering length density ρ. If the value for ρ on both sides of the film is the same one might encounter a situation as pictured in Figure 2, $\Delta\rho$ being the difference in scattering length densities between the continuous medium and the film. The physically somewhat unrealistic assumption of a steplike change of the scattering length density ρ across the border between the continuous medium and the surfactant film, as shown in Figure 2a, would cause strong oscillations in the scattering patterns which are not observed. On the contrary, the scattering curves are perfectly smooth. This suggests that we can assume that the scattering density profile $\rho(z)$ varies quite smoothly as indicated on Figure 2b. Physically this is caused by thermal disorder and the penetration of the molecules of the continuous media into the surfactant film.

With the assumption of a smooth scattering length density profile and the above relations for A and δ the expression for the scattering intensity takes the form (see Appendix, eq A7)

$$I(q) = \frac{4\pi}{\nu}\phi_s \frac{v_s}{a_s} \frac{(\Delta\rho)^2}{q^2} e^{-q^2t^2} \qquad (1)$$

The Porod Limit of a Diffuse Interface. In the case of different scattering length densities of water and oil in microemulsions, there will be a continuous transition of ρ across the interface. The

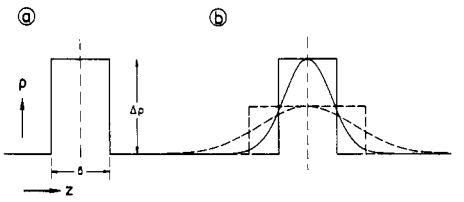

Figure 2. Possible variation of the scattering length density ρ across the amphiphilic layer in the direction of the normal z: (a) idealized rectangular profile; (b) smooth profile assumed to be Gaussian conserving the total contrast. The dashed lines represent a situation were not even in the middle of the layers the full contrast $\Delta\rho$ is reached. δ is the effective "dry" thickness with all solvent excluded from the layer.

often-observed characteristic q^{-4} decay is caused by an abrupt change of the scattering length density, known as the Porod limit.[14] If the interface, however, is diffuse (similarly as assumed above for film contrast), one may treat the local variation of the scattering length density as a step profile convoluted with a smoothing function.[16] Following Ruland and others[16-18] we chose a Gaussian smoothing function. Since the Fourier transform of a convolution product is the product of the Fourier transforms, we find for bulk contrast

$$I(q) = 2\pi\phi_s \frac{a_s}{v_s} \frac{(\Delta\rho)^2}{q^4} e^{-q^2t^2} \qquad (2)$$

Equation 2 transforms into the usual Porod limit if $t \to 0$. The exponential term leads to a steeper decay than q^{-4}. Such decays have been observed for diffuse polymer interfaces.[17,18] A priori one might expect the thickness parameter t_{bulk} of the Porod regime to be somewhat smaller than that of the film, t_{film}, because one may imagine the changes in scattering length density to occur over a fraction of the molecular length of the surfactant molecule, if for instance both the oil and the surfactant are protonated.

Empirically Observed Functional Forms. As we shall show below, the large-q part of the experimental data may be described empirically by

$$I(q) = cq^{-2}e^{-q^2t^2} + b \qquad (3)$$

in the case of film contrast, and by

$$I(q) = cq^{-4}e^{-q^2t^2} + b \qquad (4)$$

in the case of bulk contrast. Interpreting the results, the parameter c may be identified by the prefactors in eqs 1 and 2, respectively, while b is a mostly incoherent background.

Experimental Section

Materials and Phase Diagrams. n-Octane, C_8H_{18}, (>99.5%) was purchased from Merck (Darmstadt) and C_8D_{18} (>99.0%) from Cambridge Isotopes (Cambridge, MA), D_2O (>99.75%) from Merck, and n-dodecyl pentaoxyethylene glycol ether, $C_{12}E_5$ (>99%) from Nikko (Tokyo). All substances were used as purchased. In particular, for the case of measurements on the binary system water–$C_{12}E_5$, the absence of hydrophobic impurities[19] was ensured by measuring T_c, which was found to be 31.9 °C. We studied the binary system D_2O–$C_{12}E_5$ and the ternary system including deuterated n-octane. The phase diagram for the binary system is contined in ref 7 (Figure 3) and for the ternary system in ref 2 (Figure 3). The original phase diagrams were

(14) Porod, G. In *Small Angle X-ray Scattering*; Glatter, O., Kratky, Eds.; Academic Press: New York, 1982.
(15) Ibel, K. *J. Appl. Crystallogr.* **1976**, *9*, 296.
(16) Ruland, W. *J. Appl. Crystallogr.* **1971**, *7*, 383.
(17) Hashimoto, T.; Todo, A.; Itoi, H.; Kawai, H. *Macromolecules* **1977**, *10*, 377.
(18) Koberstein, J. T.; Morra, B.; Stein, R. S. *J. Appl. Crystallogr.* **1980**, *13*, 34.
(19) Schubert, K.-V.; Strey, R.; Kahlweit, M. *J. Colloid Interface Sci.* **1991**, *141*, 21.

determined by using H_2O. We found that when using D_2O the temperatures were lower by about 2 K. Otherwise the phase diagrams are practically identical. Volume fractions were calculated by using the known densities for H_2O (0.998), D_2O (1.105), octane-*h* (0.703), octane-*d* (0.814), and $C_{12}E_5$ (0.967) at 20 °C, and the molecular volume of $C_{12}E_5$ was taken as v_s = 698.3 Å^3. The weight fraction γ of $C_{12}E_5$ and the oil-in-water plus oil ratio α are given in weight percent.

SANS Measurements. Scattering experiments were carried out on the spectrometers D11 and D17 at the ILL, Grenoble. The q ranges covered were $0.0015 < q < 0.2$ and $0.01 < q < 0.36$ Å^{-1} for D11 and D17, respectively. The resolution is influenced by various factors. The main and limiting contribution, however, is the wavelength spread. The mean neutron wavelength was 10.0 Å accurate to better than 1%. The shape of wavelength distribution[15] is intermediate between a Gaussian and triangular one characterized by the full width at half-height of $\Delta\lambda/\lambda$ = 9% and 10% on D11 and D17, respectively. The other factors, like beam collimation, effective pixel size, radial averaging, etc., were adjusted as not to limit the resolution.

Temperature control was ensured by a homebuilt thermostated 15-position cell holder. The cell holder is thermostated by a digitally set thermostat (Lauda RK 20). The cell holder is made from solid aluminum, the thermostating liquid circulating back and forth through the block. This ensures temperature equilibration within the block. The actual temperature was read on two independent, absolutely calibrated Pt 100's (Newport) mounted in scattering cells. It could be set on the thermostat with an accuracy of 0.1 K but was typically constant within 0.03 K within the cells. The cell holder was mounted on a bayonet-type fitting so that it could easily be lifted and tilted. This was necessary in order to be able to mix the phases thoroughly after phase separation. The homogeneity of the mixtures was ensured always by inspection in transmitted light. If necessary the mixtures were homogenized in a separate water bath and then rapidly transferred to the cell holder.

Data Treatments. The detector sensitivity was determined by measuring the incoherent scattering of H_2O with sufficiently good statistics for the short distances. Calibration factors for the other distances were calculated from short water runs at each sample-to-detector distance. The efficiency of the individual cells of the 64 × 64 pixel 2-D detector was found to be quite uniform. Bad cells and spurious scattering around the outside rim of the detector and around the beamstop were eliminated by appropriate masking. The raw data were masked, and radially averaged and normalized by using the standard software provided by the ILL. In particular, the scattering of an empty cell was subtracted from the sample and the H_2O scattering curves taking into account the appropriate transmission factors. The data were put on absolute scale by dividing by the scattering of H_2O. Finally, the absolute scaled parts of the scattering curves, one for each sample-to-detector distance, were then combined for each sample into a single file. In the range of overlap, the data were spliced together, the splicing factor being close to unity in all cases with a possible deviation of the order of 10%. The coherent scattering component of the differential cross section per unit volume is referred to as $I(q)$ in units of cm^{-1}.

Results

Pure solvents are known to exhibit a flat scattering pattern and may serve as reference solutions. Therefore, we measured the scattering from pure D_2O and protonated *n*-octane, C_8H_{18} shown in Figure 3.

One observes that the detector response is flat and uniform down to the order of 10^{-3} cm^{-1}.

Next a typical scattering curve from the L_3 phase in the D_2O–$C_{12}E_5$ system (ϕ_s = 0.0702) is shown for comparison in Figure 3. For data analysis the precise determination of the background is important. Extending the q range to sufficiently large q one observes that the background is similarly flat as for the pure solvents. The full line is a fit of eq 3 (for details see below) demonstrating that within experimental scatter eq 3 is obeyed.

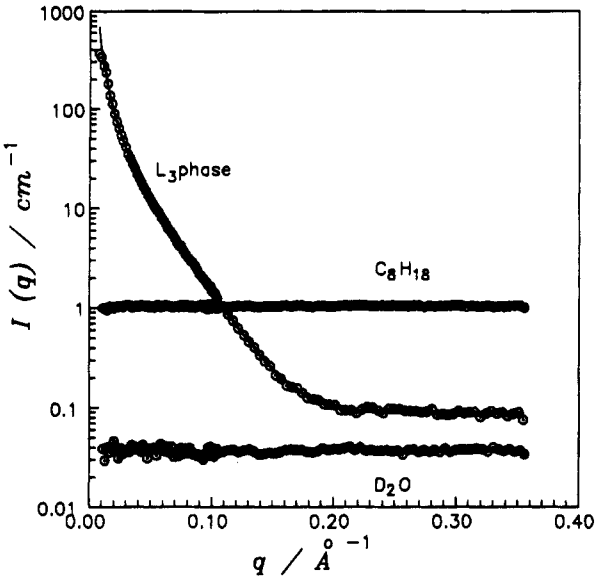

Figure 3. Scattering curves log $I(q)$ vs q of pure solvents *n*-octane and D_2O and a L_3 phase. Full lines are fits of eq 3 to the data (see Table I). Note the accurate fit over the full q range, in particular for $0.1 < q < 0.2$ Å^{-1}.

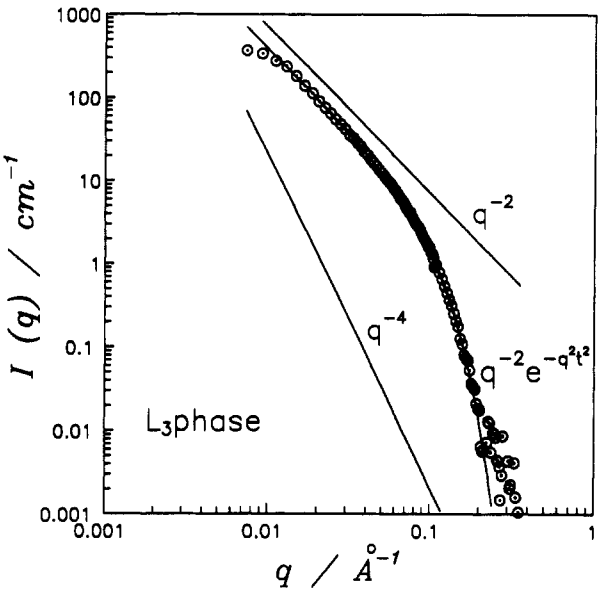

Figure 4. Scattering curve log $I(q)$ vs log q of the L_3 phase of Figure 3 with background subtracted. The full line is the fit of eq 3 (with $b = 0$). Note the steep decay at large q, significant due to the accurate determination of background scattering (cf. Figure 3). For comparison, decays proportional to q^{-2} and q^{-4} are indicated.

This permits an accurately determined background to be subtracted from the data.

Figure 4 shows the L_3 phase data of Figure 3 with the background subtracted on a log–log scale. Again the full line is the fit of eq 3 to the data (with $b = 0$). For the fit parameters and compositions of this and the following samples see Table I.

The analogous procedure has now been carried out for two samples shown in Figure 5. We show a comparison of the scattering from a monolayer and a bilayer structure as observed for a bicontinuous microemulsion and an L_3 phase, respectively. For the microemulsion the oil and water were both deuterated. In both cases we therefore have film contrast only. As one can see, the shape of the curves is in every respect similar. The full lines are fits of eq 3 (with $b = 0$).

In order to minimize experimental errors, the curves were both measured on D11 on the same day. The data normalization was performed under identical conditions. Therefore, any uncertainties in the normalization and other constants can be eliminated building

TABLE I: Compositions of the Investigated Samples and Fit Parameters According to Eq 3 (S4 and S18Lα to Eq 4) for Various Scattering Curves in the D_2O–Octane-d–$C_{12}E_5$ System (S4 and S18Lα Octane-h)[a]

sample	c	b	t	α	γ	ϕ_s
D_2O		0.037		0	0	0
C_8H_{18}		1.04		100	0	0
S28L3	3.96×10^{-2}	0.088	10.4	0	6.20	0.0702
S27L3	5.10×10^{-2}	0.14	9.8	0	8.00	0.0904
S26L3	6.49×10^{-2}	0.15	10.2	0	10.93	0.123
S24L3	1.06×10^{-1}	0.24	10.0	0	18.00	0.201
S44	1.08×10^{-2}	0.13	7.0	43.2	4.94	0.0489
S4	1.32×10^{-4}	0.63	6	38.9	5.20	0.0488
S41	7.72×10^{-3}	0.08	6.8	15.5	3.09	0.0333
S47	7.46×10^{-3}	0.11	6.5	84.7	4.53	0.0410
S18Lα	5.35×10^{-4}	0.77	6	38.9	15.88	0.150
S20Lα	3.71×10^{-2}	0.20	6.5	42.4	15.10	0.150

[a] α and γ are given in wt %. The actual surfactant volume fractions of interfacial surfactant, ϕ_s^m, for samples 44, 41, 47, and 20 are 0.041, 0.030, 0.029, and 0.144, respectively. They are smaller than the ϕ_s given in the table due to monomeric solubility of $C_{12}E_5$ in the octane estimated to be about 1.5 wt % around 30 °C.

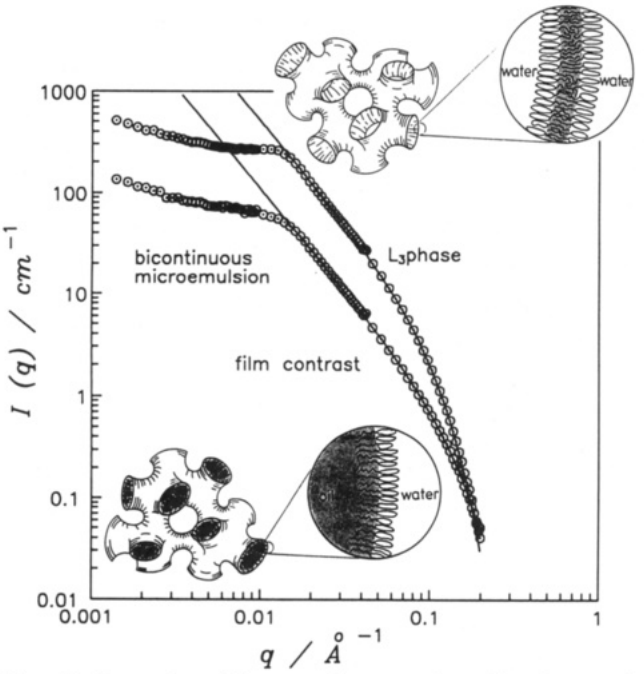

Figure 5. Comparison of the scattering curves for a bicontinuous microemulsion in film contrast and an L_3 phase determined with identical experimental setup. Note the striking similarity in the small-q part $q < 0.01$ Å^{-1}, the q^{-2} decay at intermediate q. Also note that both curves show a steep decay at large q. For the L_3 phase the decay starts, due to the larger thickness of the bilayer, at relatively smaller q than for the monolayer in the microemulsion. The insets are supposed to illustrate the topological similarity as well as the imagined local structures of the amphiphilic layers.

the ratio of the two curves, or more precisely of the parameters c obtained from fitting eq 3 to the data points. This will be done below.

Another comparison is performed by the experiment shown in Figure 6.

We compare the scattering from a bicontinuous microemulsion in film and bulk contrast measured on D11. The microemulsion contained equal volumes of water and octane and $\phi_s = 0.049$. Again building the ratio of the fit parameters c in eqs 3 and 4 should minimize the experimental uncertainties. The full lines are fits of eqs 3 and 4 to the film and bulk contrast sample, respectively.

The corresponding comparison for the lamellar phase is shown in Figure 7. It is feasible for this system[2] to enter the lamellar phase by simply increasing ϕ_s to $\phi_s = 0.15$ at constant T. The results were measured on D17 permitting also a cross check

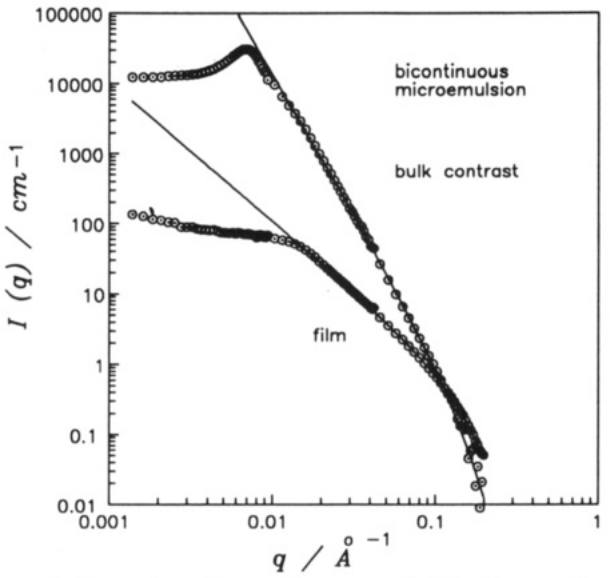

Figure 6. Comparison of scattering curves of a bicontinuous microemulsion at equal volume fractions of water and oil in bulk and film contrast. Note the q^{-4} and q^{-2} decay over several decades for bulk and film contrast, respectively, turning into even steeper decays at larger q due the diffuseness of the interfaces.

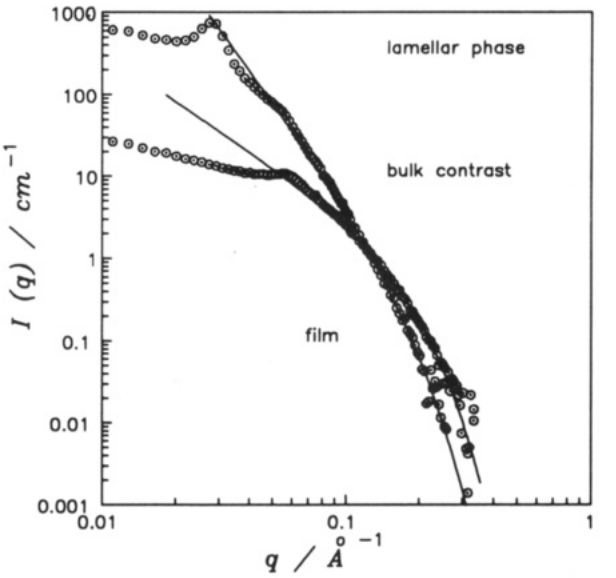

Figure 7. As for Figure 6. Powder spectrum of dilute lamellar phase. The Bragg peaks indicate a repeat distance of 225 Å for the bulk (oil or water repeat distance) and 114 Å for the films (oil and water matched).

between the different instruments.

One notes that the repeat distance of the monolayers is about one-half that of the bulk oil–water repeat distance, as one would expect, because there are two monolayers per water or oil layer.

Discussion

The evaluation is carried out in two steps. First, we show that a model-free empirical description yields two parameters c and t which in a second step under the assumption of diffuse interfaces can be related to the molecular properties of interfacial layers.

Empirical Description. Having determined and subtracted the background one observes, experimentally, on a log–log scale in Figure 4 that the scattering turns from a q^{-2} dependence at small q into a steep decay with increasing q, even steeper than q^{-4}. The experimental results alone suggested an empirical description in terms of a three parameter fit. Equation 3 is found to fit the data points reasonably well (see Figures 3–7). In the low-q limit deviations start to occur when $q/2\pi$ becomes of the order of the tubular diameters (see Figure 1 and inset of Figure 5). Considering Figure 4 one finds that in the large-q limit the scatter of

the data becomes so large that we consider data for $I(q) < 10^{-2}$ cm^{-1} to be no longer significant, presumably due to the unevenness of the detector and counting statistics.

We have studied the scattering of samples in the L_3 phase as it depends on the total surfactant concentration. The data are very similar to those shown in Figure 4. The corresponding fit results are summarized in Table I. In particular, the background increases systematically as the surfactant concentration is increased. The reason presumably may be found to a large extent in the increasing incoherent scattering with increasing total hydrogenated compound in the mixtures. The total scattering intensity scales with ϕ_s. These results support and extend the results of a previous study on the same system.[7] In that study, however, a poorer scattering statistics at large q had not permitted the observation of the essentially smooth scattering profile instead of the anticipated $\sin^2(q\delta/2)/(q\delta/2)^2$ variation.

For the case of bulk contrast in microemulsions the theoretical arguments leading to eq 2 presented above suggested to empirically try eq 4. We have fitted eq 4 to a number of dilute microemulsions, including droplet microemulsions to be discussed in a forthcoming paper, and found that indeed there is a steeper decay than q^{-4} also in bulk contrast at large q. The results pertinent to this paper are shown on Figures 6 and 7. The parameters are included in Table I.

Diffuse Interface Description. In an attempt to theoretically explain the steep decay at large q we have assumed that the scattering length density varies smoothly, instead of an abrupt change which would cause a q^{-4} decay[14] even for a thin platelike object. The experimentally found functional form of eqs 3 and 4 suggests that assuming a Gaussian scattering length density distribution along the normal of the layers is a reasonable description. As detailed in the Appendix, the Gaussian scattering length density variation exactly yields the functional form of eq 3. From the fit results we obtain a mean value for the thickness parameter $\bar{t} = 10.1$ Å. If the scattering length density distribution were truly Gaussian one could evaluate the effective thickness by $\delta = (2\pi t^2)^{1/2}$ and find it to be $\delta = 25.3$ Å and $a_s = 55.2$ Å^2 per molecule in the bilayers of the L_3 phase of the binary system water–$C_{12}E_5$. This value for a_s, however, relies on the validity of the assumption of a strictly Gaussian profile which may be a too simplified description. If, however, we compare eqs 1 and 3 we see that the parameter c is given by $c = 4\pi\phi_s v_s(\Delta\rho)^2/a_s$. For the L_3 phase samples we find a mean value $a_s = 62 \pm 3$ Å^2, irrespective of the assumption on the exact profile. This value relies only on the accuracy of the absolute calibration of the intensity and on $(\Delta\rho)^2$ taken as $(\Delta\rho)^2 = 3.83 \times 10^{21}$ cm^{-2}.

The scattering from the monolayer shown in Figure 5 is strikingly similar to that of the bilayer of an L_3 phase: In both cases one observes a q^{-2} decay which with increasing q monitors the thickness of the film modified by the diffuse nature of the interface. The amphiphile concentrations were chosen such that about the same amount of total internal surface is formed. Therefore, going toward low q one observes at about the same q a shoulder or soft bump. At even lower q the scattering in the two phases is again strikingly similar, supporting the notion of the topological similarity of bicontinuous microemulsions and the L_3 phases. While the topological question is of considerable interest we confine ourselves here to the local structure monitored by the large-q part of the curves.

Considering the predictions of eq 1 for mono- and bilayer scattering, we have for ratio of the prefactors

$$\frac{c_m}{c_b} = \frac{1}{2}\frac{\phi_s^m a_s^b (\Delta\rho)_m^2}{\phi_s^b a_s^m (\Delta\rho)_b^2} \tag{5}$$

where the sub- and superscripts m and b stand for mono- and bilayer, respectively. We note that the effect of the different thicknesses enters the ratio through volume conservation (see derivation of eq 1 above). Evaluating eq 5 for the curves shown in Figure 5, we find setting tentatively $a_s^m \approx a_s^b$ that $\Delta\rho_m = 0.97\Delta\rho_b$. This finding implies that the penetration of solvent molecules into the surfactant film for the monolayer is insufficient to lower the contrast significantly below its maximum $\Delta\rho$. The value of $t_m = 7$ Å is somewhat larger than the 5 Å one expects from half a bilayer. Therefore, one might expect the surfactant tails in the bilayers to mutually interdigitate. Similar t_m values are found for measurements on samples with different water-to-oil ratios and even droplet microemulsions.

Comparing the scattering of the monolayer and the bulk in the Porod limit we find from eqs 1 and 2

$$\frac{c_m}{c_{bulk}} = \frac{(\Delta\rho)_m^2}{(\Delta\rho)_{bulk}^2}\frac{v_s^2}{(a_s^m)^2} \tag{6}$$

where the subscript bulk stands for bulk contrast. This ratio is sensitive to the actual value of the area per surfactant molecule because all other constants cancel out. Evaluating eq 6 for the curves shown in Figure 6 we find $a_s^m = 69.7$ Å^2 assuming that we have full contrast in the middle of the monolayers as was suggested by the comparison in eq 5 above. The analogous evaluation for lamellar samples (Figure 7) yields $a_s^m = 75.7$ Å^2. We emphasize that the particular model of a diffuse interface merely serves to precisely extract the parameter c and does not have an influence on the actual values of a_s.

Accuracy and Significance of the Results. Sources of error are the finite resolution, the absolute calibration of the data, the sample preparation, and precise temperature control. We have checked the effect of the neutron wavelength distribution. For that purpose we have integrated the calculated scattering profiles over the actual triangular wavelength distribution (see Experimental Section). However, the effect was hardly noticeable. The tendency is to reduce the parameter t by a few percent and therefore has a negligible influence on the actual figures presented.

The parameter c in Table I relies on the accuracy of the absolute calibration. Building the ratios in eqs 5 and 6, however, this uncertainty drops out because the compared scattering curves were measured under identical conditions. What remains are the errors in the transmission measurements, estimated to be about ±3%.

The experiments shown in Figures 6 and 7 were performed on different instruments. Yet, they practically yield the same result: the mean area per surfactant molecule is 72 Å^2 in the monolayer. Therefore, also the following observation is significant: The scattering peak in Figure 7 of the lamellar phase yields a characteristic distance of $D_{Bragg} = 225$ Å. From the area of the surfactant molecules obtained from the same curve at large q one would expect a $D_{Bragg} = 129$ Å. Thus, we calculate from the spacing an apparent total internal area smaller by a factor 0.57. Strongly undulating monolayers separating water and octane would cause such an area deficit. An alternative would be in invoke a considerable number density of area consuming defects. A similar observation had already been made by Lichterfeld et al.[20] on the related system water–tetradecane–$C_{12}E_5$. If one, tentatively, would assume strictly flat monolayers, the area a_s would have to be 41 Å^2, inconsistent with what we found above from building the ratio between bulk and film scattering. Thus, we conclude that the evaluation of surfactant areas from structure factor maxima may be in error for dilute lamellar phases due to the undulating nature of the surfactant layers or due to small defects such as passages.[8,11] In a recent study[7] on the dilute lamellar phase of the binary system water – $C_{12}E_5$ an explanation in terms of a logarithmic area correction had been suggested. However, the large deficit observed here for the ternary system seems somewhat large to be solely attributable to undulations.

Structure Factors. In preceding publications[2,22] we have reported on the evolution of the ubiquotiuos scattering peak[21] in microemulsions with changing water-to-oil ratio and surfactant concentration observed in bulk contrast. Also the peak shown in Figure 6 is well described by the formula given in ref 21.

(20) Lichterfeld, F.; Schmeling, T.; Strey, R. *J. Phys. Chem.* **1986**, *90*, 5762.
(21) Teubner, M.; Strey, R. *J. Chem. Phys.* **1987**, *87*, 3195.
(22) Magid, L.; Butler, P.; Payne, K.; Strey, R. *J. Appl. Crystallogr.* **1988**, *21*, 832.

The soft bump or shoulder in the film scattering curves is less well understood. We only note here that apparently for a variety of different L_3 phases very similar curves are obtained.[5-7] The soft bump in the film scattering observed in microemulsions (see Figure 6) is directly correlated with the peak in bulk contrast[23] and corresponds to the tubular diameter (see Figure 1).

The surprising similarity of the scattering curves shown on Figure 5 at q smaller than 0.01 Å^{-1} indicates a very similar spatial arrangement of the bilayer in the L_3 phase and in the monolayers in the bicontinuous microemulsions. Since in the latter the monolayer is continuously connected (water–oil contact is very unlikely) we expect this also to be the case for the L_3 phase from scattering by analogy. Freeze fracture electron microscopic results[4,8] support the insets in Figure 5. Scattering alone cannot decide whether earlier suggestions of large disconnected disklike micelles as structure elements[24,25] are ruled out as a structural alternative. From recent NMR self-diffusion experiments, however, Balinov et al.[26] concluded that the probable L_3 phase structure is one as pictured in Figure 1 for a broad range of surfactant concentrations.

In discussing our results we find support for the notion of fluctuating interfaces[27] governing the microstructure and phase behavior of microemulsions and L_3 phases. Undulations and passages seem an indispensable characteristic of these solutions of fluid membranes.

In a subsequent paper we will apply the diffuse interface description to well-defined droplet structures. Furthermore, we are studying a number diferent shapes, e.g., locally near-spherical, cylindrical, and planar structures into which the surfactant films can be tuned by temperature variation at constant composition in the ternary water–oil–nonionic surfactant system.

Conclusions

Analyzing the large-q part of the SANS spectra we observed a characteristic deviation from the usual q^{-2} and q^{-4} behavior of film and bulk scattering, respectively. The deviation was in all cases to decrease the intensity of the large-q part dramatically. Following ideas of Ruland[16] and Porod[14] we exploited the notion of a smooth scattering length density profile across the films.

We conclude that the local structure of monolayers of $C_{12}E_5$ in the microemulsion is characterized by a considerable penetration of water and octane into the surfactant film. This penetration causes the scattering length density to vary smoothly across the monolayer. It can be described by a Gaussian distribution with a thickness parameter $t = 7$ Å. The area per surfactant molecule we find to be $a_s = 72 \pm 3$ Å^2.

Due to the strong hydration of the surfactant headgroups by penetrating water molecules the local structure of the bilayers of the L_3 phase is similarly characterized by a thickness parameter $t = 10$ Å of the Gaussian density profile. Such a low value suggests that the hydrocarbon tails of the surfactant molecules form an about 10 Å thick hydrocarbon-rich film in which the tails from the opposing monolayers intimately interdigitate. From absolute calibration we find the area per surfactant molecule in the bilayer samples to be $a_s = 62 \pm 3$ Å^2. The absolute calibration itself is uncertain by about 10%.

Speculating, one might interpret the first experimental hint for an interdigitation of the surfactant tails in this system as the origin of the surprisingly high swelling observed[7] for the L_3 and lamellar phase in the binary system water–$C_{12}E_5$.

The above-quoted values for areas of surfactant molecules in mono- and bilayers are larger than what has been considered in calculating bending properties of single-chained surfactant layers.[28] In particular, the high degree of penetration of solvent molecules, hitherto neglected, should possibly be taken into account. Furthermore, the possibility of interdigitation of the two monolayers comprising the bilayer deserves consideration as well.

Acknowledgment. We are indebted to Prof. M. Kahlweit for his support and encouragement. Useful discussions with M. Teubner and U. Olsson are gratefully acknowledged. R.S. thanks D. Roux and G. Porte for introducing him into field of undulating membranes. Partial support by the European Community is acknowledged. L.M. acknowledges the support of the U.S. National Science Foundation. We also thank our local contacts at ILL, K. Ibel, P. Lindner, and B. Farago.

Appendix

Here we derive the scattering of a locally flat structure with a smooth scattering length density profile. Following Porod,[14] we write for the scattering of a single (thin) plate

$$I_1(q) = A\frac{2\pi}{q^2}I_t \tag{A1}$$

with A being the area of the plate and

$$I_t = F_t^2 \tag{A2}$$

We need expressions for A and $I_t(q)$. As long as the plates are randomly oriented in space the scattering intensities will add. The amplitude F of the scattering is proportional to the difference in scattering length density ρ. The experimental results suggest that we can assume that the scattering density profile $\rho(z)$ varies quite smoothly as indicated on Figure 2b. with the condition that the total contrast is preserved

$$\Delta\rho\delta = \int_{-\infty}^{+\infty} \rho(z)\, dz \tag{A3}$$

For simplicity we assume a Gaussian profile

$$\rho(z) = \Delta\rho e^{-z^2/(2t^2)} \tag{A4}$$

with $\delta = (2\pi t^2)^{1/2}$, because $(2\pi t^2)^{-1/2}\int_{-\infty}^{+\infty} e^{-z^2/(2t^2)}\, dz = 1$. As pointed out by Porod,[14] due to the planar symmetry the three-dimensional Fourier transform is reduced to a one-dimensional cosine transform

$$F_t(q) = \int_{-\infty}^{+\infty} \rho(z) \cos qz\, dz = \Delta\rho\, \delta e^{-q^2t^2/2} \tag{A5}$$

Inserting (A5) in (A2) we have

$$I_t = (\Delta\rho)^2\delta^2 e^{-q^2t^2} \tag{A6}$$

and (A6) in (A1) we have

$$I_1(q) = A\frac{2\pi}{q^2}(\Delta\rho)^2\delta^2 e^{-q^2t^2} \tag{A7}$$

For comparison we quote the result for a rectangular ρ distribution (Porod,[14] p 35)

$$I_1(q) = A\frac{2\pi}{q^2}(\Delta\rho)^2\delta^2 \sin^2(q\delta/2)/(q\delta/2)^2 \tag{A8}$$

Thus $I(q)$ in eq A7 shows no minima due to the $\sin^2(q\delta/2)/(q\delta/2)^2$ term as would result from the usual assumption of a rectangular ρ distribution, because of the Gaussian distribution (eq A4) of the scattering length density. Furthermore, we note that expanding eqs A7 and A8 one finds that in the Guinier regime a significantly slower decay with increasing q is observed, whereas for very large q a steeper decay than q^{-4} is observed.

Obviously there are two regimes: For $q^2t^2 \ll 1$ one finds I proportional to q^{-2} from which one may obtain $A(\Delta\rho)^2\delta^2$. For $q^2t^2 \sim 1$ one has $\ln(Iq^2)$ proportional to $-q^2$ with slope t^2, the effective width of the smooth scattering length density region. We note, having followed ourselves a more conventional derivation,[14] that Teubner[29] gave recently a general treatment on the scattering from two-phase random media.

Registry No. $C_{12}E_5$, 3055-95-6; octane, 111-65-9.

(23) Teubner, M. *Europhys. Lett.* **1991**, *14*, 403.
(24) Nilsson, P. G.; Lindman, B. *J. Phys. Chem.* **1984**, *88*, 4764.
(25) Miller, C. A.; Gosh, O. *Langmuir* **1986**, *2*, 321. See also: Miller, C. A.; Gradzielski, M.; Hoffmann, H.; Krämer, U.; Thunig, C. Proceedings of the ECIS Conference 1990. *Prog. Colloid Interface Sci.*, in press.
(26) Balinov, B.; Olsson, U.; Söderman, O. *J. Phys. Chem.*, in press.
(27) Golubovic, L.; Lubensky, T. C. *Phys. Rev.* **1990**, *A 41*, 4343.
(28) Szleifer, I.; Kramer, D.; Ben-Shaul, A.; Gelbart, W. M.; Safran, S. A. *J. Chem. Phys.* **1990**, *92*, 6800.
(29) Teubner, M. *J. Chem. Phys.* **1990**, *92*, 4501.